数理解析研究所講究録
1496巻 2006年 151-158

乱流中のパッシブスカラー場の間欠性と散逸場の構造について

名古屋工業大学大学院機能工学専攻 渡邊 威 (Takeshi WATANABE) watanabe@nitech.ac.jp
後藤 俊幸 (Toshiyuki GOTOH) gotoh.toshiyuki@nitech.ac.jp
Department of Engineering Physics, Nagoya Institute of Technology

1 Introduction

The fundamental issue of study of passive scalar turbulence is to clarify the statistical nature of intermittency in a scalar field. Passive scalar intermittency has been captured by the scaling laws of structure function for the scalar increment $\delta\theta_r = \theta(\mathbf{x}+\mathbf{r}) - \theta(\mathbf{x})$ in the inertial convective range (ICR) as

$$\langle(\delta\theta_r)^q\rangle \sim r^{\zeta_q^\theta} \quad (\bar{\eta} \ll r \ll L). \tag{1}$$

Obukhov-Corrsin scaling law $\zeta_q^\theta = q/3$ was suggested by the dimensional arguments [1, 2]. However many experimental or numerical results do not follow it and shows the values smaller than $q/3$, and so does the velocity case ζ_q^u [3].

A central importance of passive scalar intermittency is universality of ζ_q^θ. In order to discuss this problem more carefully, it is effective to change large scale conditions of the scalar alone while keeping the turbulent velocity field the same and to see the difference in the scalar statistics. Recent DNS studies in this direction lead to the remarkable results that ζ_q^θ is insensitive to the variation of large scale injection schemes, Gaussian white random source (case R) or uniform mean scalar gradient (case G), in the case for 2D passive scalar convected in the energy inverse cascading range [5, 6], while the case of 3D is dependent of the injection scheme for both cases [7, 8]. The former is in favor of the predictions of the Kraichnan model [9] in spite of the intrinsic differences in the correlation time of the velocity field, and bears the expectation that ζ_q^θ evaluated in the generic turbulent flow is universal [10, 11]. However the latter implies that universality based on the zero mode idea should be extrapolated to 3D passive scalar intermittency with some care [8]. Here we summarize the points raised in 3D results [8] as follows.

1. $\zeta_q^{\parallel} \simeq \zeta_q^{\perp}$ for case G (Fig.1), where $\parallel$ ($\perp$) denotes the parallel (perpendicular) component of structure function to the direction of mean scalar gradient.
2. ζ_q^G ($= \zeta_q^\theta$ for case G) and ζ_q^R (for case R) with large q saturate about $\zeta_\infty^\theta = 1.3$ and 1.5, respectively. Then the PDF tails of the scalar increment is well fitted by the one point scalar PDF (Fig.2) as

$$P(|\delta\theta|, r) = \frac{(r/L)^{\zeta_\infty^\theta}}{\sqrt{2}} P_\theta\left(\frac{|\delta\theta|}{\sqrt{2}}\right) \quad (|\delta\theta| > 4\theta_{rms}). \tag{2}$$

3. $\zeta_q^G < \zeta_q^R$ (Fig.1), i.e. case G is more intermittent than case R.

The third point is in sharp contrast to the results by DNS in 2D [5, 6] and by the theoretical suggestion [10, 11]. What is the origin of this discrepancy? Although the possible reasons were discussed in [8], it is very difficult to draw the definite conclusions from the present DNS resolution.

Saturation of ζ_q^θ is regarded as the extreme case of intermittent nature of the dissipation field because it is closely related to the ramp-cliff structures observed in the scalar field [3]. Relation (2) represents that the high order statistics of $\delta\theta_r$ is dominated by the rare events encompassing the large jump of θ (cliff) residing in small region. Then the prefactor $(r/L)^{\zeta_\infty^\theta}$ in eq.(2) means the probability to find a cliff in separation distance r. This is also explained in terms of the spatial distribution of cliff and represented by its geometrical dimension μ as $(r/L)^{3-\mu}$. That is, $\mu = 3 - \zeta_\infty^\theta$. If the scaling exponent ζ_q^θ is dependent of the scalar injection mechanism at large scale, we expect that the geometric feature of the scalar dissipation is also affected by the large scale conditions.

Main purpose of the present study is to clarify the three points raised above in terms of the dissipation field statistics. The geometrical dimensions of intense structures of velocity and scalar gradient fields are computed from the DNS data, as done by Moisy and Jiménez [12]. We discuss the relation between the

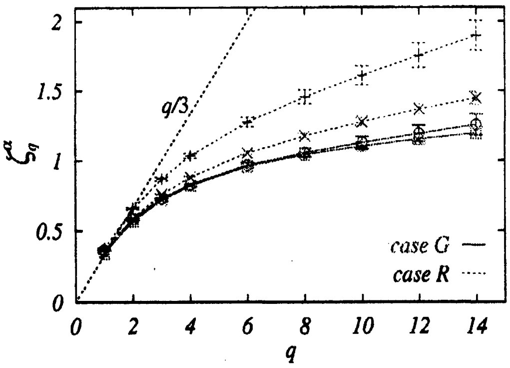

Figure 1: The scaling exponents for case G (circles; $\zeta_q^{\parallel}$, squares; $\zeta_q^{\perp}$) and case R (plus signs; ζ_q^R in ICR, crosses; ζ_q^R in VCPR), respectively.

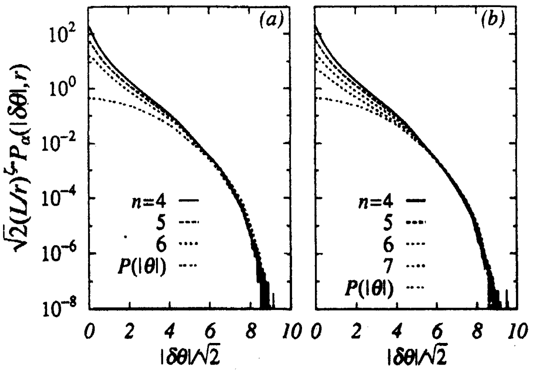

Figure 2: Scaling plots of scalar increment PDFs with $\zeta_\infty^\alpha = 1.3$ for the PDFs of (a) parallel $|\delta_{\parallel}\theta_r|$ and (b) perpendicular $|\delta_\perp\theta_r|$ components to mean scalar gradient, respectively.

geometry of the field structure and the saturation of ζ_q^θ. Moreover we analyse the effects of large scale condition on the geometrical dimension and the intermittency exponents of the moment for the locally averaged dissipation fields by performing the DNSs with the different scalar injection schemes. Several results drawn from the present studies are discussed by comparing the preceding ones.

2 Direct numerical simulations

We numerically solve the passive scalar field $\theta(\mathbf{x}, t)$ in a periodic box with periodicity 2π which obeys the advection diffusion equation convected by the velocity field of Navier-Stokes equation as

$$(\partial_t + u_j\partial_j - \kappa\partial_j^2)\theta = f_\theta, \quad (\partial_t + u_j\partial_j - \nu\partial_j^2)u_i = -\partial_i P + f_i, \tag{3}$$

where f_i is the solenoidal random force, Gaussian white in time which is applied at low wavenumber band [13]. Schmidt number $S_c = \nu/\kappa$ is fixed to be unity. The scalar source f_θ is a random Gaussian white in time [7] (case R) or a uniform mean scalar gradient in the x_3 direction (case G), $f_\theta = -Gu_3$ [8, 14], where G is a constant and fixed as $G = 1$. The detailed numerical scheme of DNS can be found in [7]. Here we show the results at $R_\lambda = 427$ (case R) and $R_\lambda = 468$ (case G) with $N^3 = 1024^3$ grid points. Five (two) instantaneous fields recorded at intervals of 0.3 (0.15) T_{eddy} were used to analyse the several statistical quantities for case G (case R).

In order to discuss the scaling properties of dissipative quantities introduced later, it is useful to determine the ICR in the present DNS. Figure 3 shows the behavior of each terms appeared in Yaglom's equation derived from eq.(3) [15] under the assumptions of statistical homogeneity and isotropy as,

$$\frac{4}{3}\bar{\chi}r = -\langle\delta u_r\delta\theta^2\rangle + 2\kappa\frac{d}{dr}\langle\delta\theta_r^2\rangle - \frac{2}{r^2}\int_0^r r'^2 G\langle\delta u_3\delta\theta\rangle\, dr'. \tag{4}$$

Relation (4) is well satisfied in the region $r/\bar{\eta} < 200$ where the isotropy is satisfied very well. The 4/3 law is also observed in $20 < r/\bar{\eta} < 200$ which is dominated by the first term of right hand side of eq.(4).

3 Geometric features of intense structures

In this section, we discuss the geometric features of intense structure extracted from the derivative fields. We define the norm of derivative fields (named by α), vorticity ω, strain s, scalar gradient g, perpendicular scalar gradient g_p, and normal scalar gradient g_n, as follows.

$$\omega = |\omega_i\omega_i|^{1/2}, \quad s = |S_{ij}S_{ij}|^{1/2}, \quad g = |\nabla\theta|, \quad g_p = |\nabla_{\parallel}\theta|, \quad g_n = |\nabla_{\perp}\theta|, \tag{5}$$

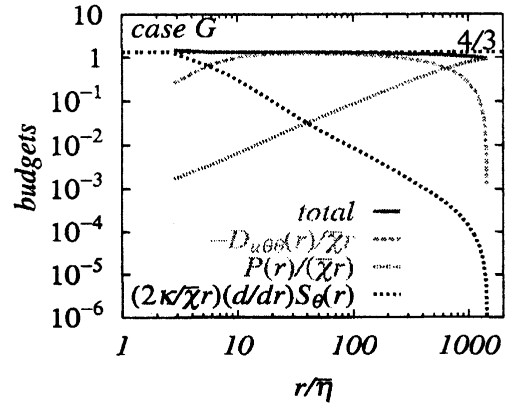

Figure 3: Variation of terms appeared in the Yaglom's equation against $r/\bar{\eta}$.

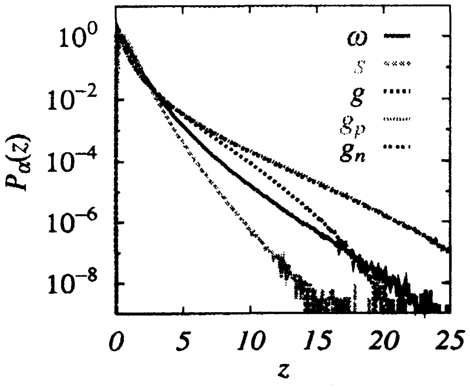

Figure 4: One point PDFs for several derivative fields defined in eq.(5)

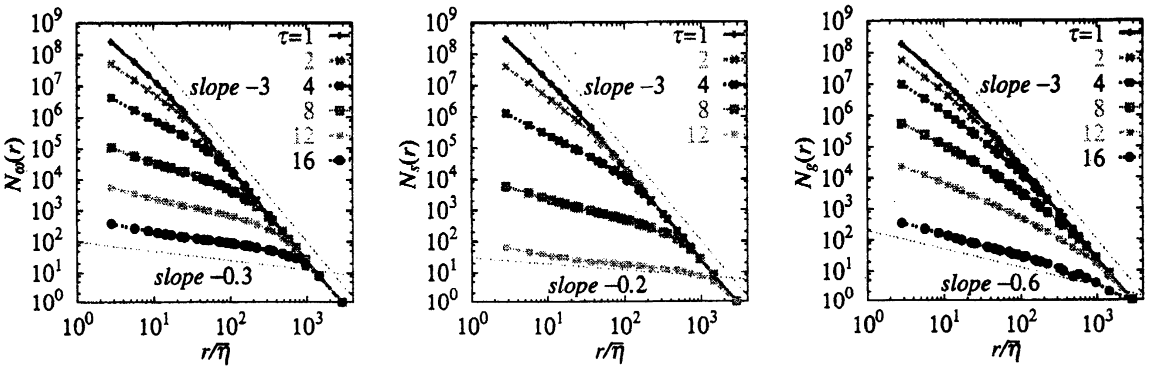

Figure 5: Variations of box number for covering level set of ω (left), s (center) and g (right) for $\tau = 1 \sim 16$ against the box size r normalized by $\bar{\eta}$.

where $S_{ij} = (\partial_j u_i + \partial_i u_j)/2$ and $\omega_i = (\nabla \times \mathbf{u})_i$ are the rate of strain tensor and vorticity vector, respectively. Figure 4 shows the one point PDFs for derivative fields in eq.(5) normalized as $z = \alpha/\alpha_{rms}$ for case G. We can see that the PDF tail of g has a large probability than that for ω and s, i.e. the scalar gradient field g is more intermittent than that of vorticity ω or strain s. Moreover it should be noted that the behavior for g_p and g_n is almost same for the whole intensity of fluctuations.

In order to characterize the geometric feature of the above-mentioned derivative fields, we investigate the box counting dimension (BCD) D_0 for the level set of intense structures extracted from the derivative fields. Scheme for performing this analysis is summarized as follows.

1. Extracting the level set from the whole domain in 3D satisfying the condition $\alpha \geq \tau\alpha_{rms}$, τ being the level parameter we control.
2. The box size $r = l\Delta x, (\Delta x = 2\pi/N,\ l = 1, 2, \cdots, N)$ is chosen to satisfy the condition mod$(N + m, l) = 0$ for integer m with $0 \leq m \leq 3$. This condition is due to the requirement for obtaining the smooth curves to determine D_0 more than the usual case as $r = 2^n\Delta x$ [12].
3. Counting the box numbers $N_\alpha(r, \tau)$ to be needed to cover level set extracted in procedure 1. for each r and τ, in which we expect the scaling behavior $N_\alpha(r, \tau) \sim r^{-D_0}$.

Figure 5 shows the variation of $N_\alpha(r, \tau)$ for $\alpha = \omega$, s and g against the box size r normalized by Kolmogorov scale $\bar{\eta}$ for each τ. We can see the trivial scaling $N_\alpha(r, \tau) \sim r^{-3}$ at larger box sizes, where the region scaled by r^{-3} decreases with increase of τ. Behavior is almost same for ω, s and g for smaller τ, while that for larger τ, the scaling behavior is clearly different for each fields, in which N_s has a smaller exponent than the others. This fact corresponds to the PDF behavior shown in Fig.4. In order

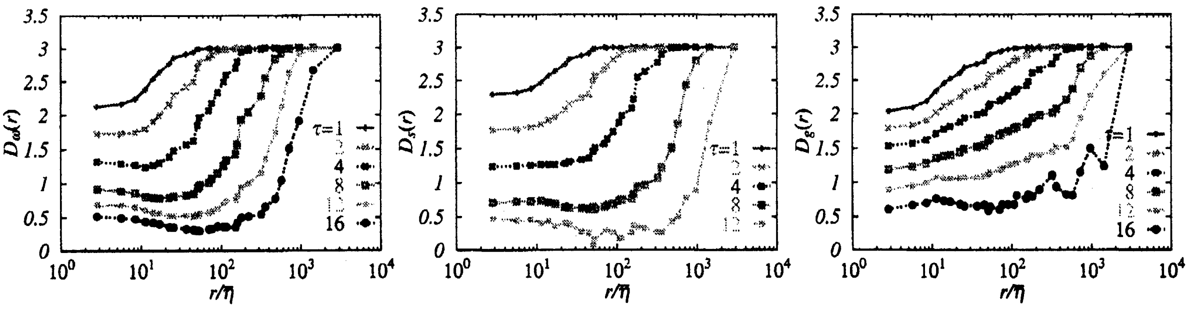

Figure 6: Variations of local box-counting dimensions evaluated by the curves in Fig.5.

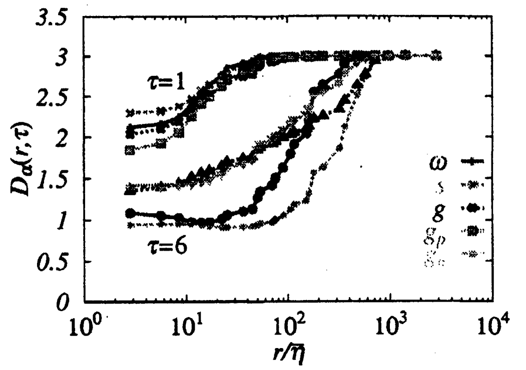

Figure 7: Comparison of local BCD for $\tau = 1$ (upper curves) and 6 (lower curves).

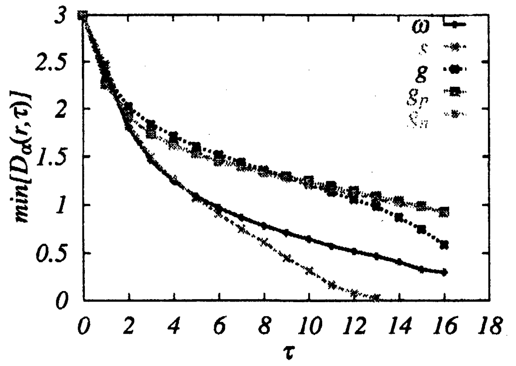

Figure 8: Variation of minimum values of local BCDs against the level set parameter τ.

to search the scaling region and to determine D_0, we compute the local BCD defined by $D_\alpha(r,\tau) = -d\log N_\alpha(r,\tau)/d\log r$. Curves for $D_\alpha(r,\tau)$ corresponding to Fig.5 are shown in Fig.6. Clear plateaus are not observed for all case of α except the trivial scaling $D_\alpha(r,\tau) = 3$ at larger r. Trends of behavior for ω and s are totally same as those by Moisy & Jiménez [12]. The behavior of D_g is clearly different from that of $D_{s,\omega}$. For ω and s, it is found that there is a local minimum which decreases with increase of τ, while the case for g, the local slopes gradually decrease as r decreases and there is no local minimum.

Figure 7 shows the comparison of $D_\alpha(r,\tau)$ for five derivative fields defined in eq. (5) at $\tau = 1$ and 6. In the case of $\tau = 1$, $D_\alpha(r,\tau)$ curves are almost same irrespective of α at $r/\bar{\eta} > 10$. This implies that the geometric feature of level set for the intensity of fluctuation larger than the average value is independent of the kind of field. In contrast for $\tau = 6$, we can see that the behavior is divided into two groups as the scalar gradient fields or the vorticity and strain ones, where the scalar gradient fields are more space filling than the vorticity and strain ones. In the range around $r/\bar{\eta} = 50$, it is estimated that $D_{\omega,s}(\simeq 1) < D_{g,g_p,g_n}(\simeq 1.5)$. This fact is also consistent with the observation of Fig.4 or $\zeta_q^\theta < \zeta_q^u$ [7].

Although $D_\alpha(r,\tau)$ curves have no plateau except $D_\alpha(r,\tau) = 3$ at larger r, the geometric feature of derivative field can be characterized by estimating the lower bound of D_0 from the curves of $D_\alpha(r,\tau)$. We evaluate minimum values of $D_\alpha(r,\tau)$, $D_\alpha^*(\tau)$, at $r/\bar{\eta} > 10$ and discuss its τ-dependences, as done by Moisy & Jiménez [12]. The limitation $r/\bar{\eta} > 10$ is due to the fact that the statistics at $r/\bar{\eta} < 10$ is contaminated by the insufficient DNS grid size to resolve the derivative field accurately [17]. Results are shown in Fig.8. As shown in Fig.7, we can clearly recognize that $D_{\omega,s}^*(\tau) < D_g^*(\tau)$ at $\tau > 2$, i.e. the scalar gradient fields are more space filling than those of velocity derivatives. While the case for $\tau < 2$, D_α^* has the values between 2 and 3 independent of α. The smaller τ structures have the larger probability, as we can see in Fig.4, the BCDs for contributing the global dissipation of the energy and scalar variance are predominated by them. Moisy & Jiménez [12] estimated $\langle D_\omega^* \rangle \simeq 2.5$ and $\langle D_s^* \rangle \simeq 2.6$ by $\langle D_\alpha^* \rangle = \int_0^\infty P(\tau) D_\alpha^*(\tau)\, d\tau$. Evaluation of them by the present results are not made because we have no accurate data for smaller τ. It should be noticed that the curve for g_p and g_n almost collapses for all region of τ. This implies that the geometric feature of scalar gradient is insensitive to the direction of mean scalar gradient and supports the observation $\zeta_q^{||} \simeq \zeta_q^{\perp}$ stated in Sec. 1.

Let us now discuss the relation between saturation of ζ_q^θ and the geometrical dimensions shown in Fig.8. As stated in Sec.1, the saturating value ζ_∞^θ is related to the geometrical dimension μ of the support of spatial distribution of cliffs as $\mu = 3 - \zeta_\infty^\theta$. How strong intensity of fluctuation does contribute to the saturating phenomenon? As stated in Sec.1, the large jump of scalar corresponds to the rare event of scalar gradient fluctuation which may be bounded by the scalar increment encompassing a mean cliff width Δ as $|\partial_z\theta| > |\delta\theta_r|/\Delta$ with $r \geq \Delta$. Mean cliff width Δ is experimentally evaluated by $\Delta = (13 \pm 3)\bar{\eta}$ [16] which is almost same as the Taylor microscale of scalar field defined by $\lambda_\theta = \theta_{rms}/\langle(\partial_z\theta)^2\rangle^{1/2} = 20\bar{\eta}$ from the present DNS. Moreover the asymptotic scaling law of PDF (eq.(2)) leading to the saturation of ζ_q^θ is observed in their rare events with $|\delta\theta_r| > 4\theta_{rms}$. Therefore we guess the inequality

$$|\partial_z\theta| > |\delta\theta_r|/\lambda_\theta > 4\theta_{rms}/\lambda_\theta = 4\sigma_{\partial\theta} \tag{6}$$

determines $\tau \simeq 4$ to discuss the relation between the saturation of scaling exponent and geometric feature of intense structures contributing the saturating phenomenon. From Fig.8, the lower bound of BCD contributing to the saturation is estimated by $D_g^*(4) \simeq 1.7$, which is quite in good agreement with the estimation $\zeta_\infty^\theta = 3 - 1.7 = 1.3$ in the second observation in Sec. 1.

There is an unsolved important problem why the scalar gradient field is more space filling than the vorticity and strain fields. As shown in Fig.8, $D_g^* - D_\omega^* \simeq 0.7$ at larger τ. This difference may be explained by the detailed analysis of the eigenvalue of the rate of strain tensor S_{ij}. We can derive the equations of motion for $\omega^2/2$, $g^2/2$, and $\omega_i g_i$ in the inviscid and force free cases as

$$\frac{D}{Dt}\frac{\omega^2}{2} = \omega_i S_{ij}\omega_j, \quad \frac{D}{Dt}\frac{g^2}{2} = g_i(-S_{ij})g_j, \quad \frac{D}{Dt}\omega_i g_i = 0. \tag{7}$$

The mechanism for amplification of ω^2 and g^2 are determined by the detailed natures of S_{ij}. Important point is that when the vorticity is amplified by the local strain, then the scalar gradient is also amplified in the direction perpendicular to the vorticity vector at the same time [18]. As expected from eq.(7), the formation mechanism of intense structures is governed by the eigenvalues of S_{ij} and the alignment between the eigenvectors and ω_i or g_i [19]. It is very interesting to clarify the relation between the spatial distributions for the intense structures of ω and g and the eigenvalue distributions with the alignment statistics. This is the future subject of the present study.

4 Examination of scalar source dependence

In this section, we investigate how the scalar injection scheme at large scale affects the geometric feature of scalar gradient field or scaling behavior of moment of the locally averaged scalar dissipation field.

4.1 Box counting dimension

We compute the BCD for case R as carried out for case G in the previous section and compare them to those by case G. Comparisons between case G and R for $N_g(r,\tau)$ and $D_g(r,\tau)$ curves are shown in Figs.9 and 10, respectively. For small τ up to $\tau = 2$, the behavior of case G are almost same as those of case R in the whole scale, which implies that the geometric feature of the scalar gradient field with small intensity of fluctuations are almost independent of the large scale injection mechanism. In contrast for $\tau > 2$, the local BCDs for case G deviate from those for case R. In the ICR of $60 < r/\bar{\eta} < 200$, we can see $D_g^R(r,\tau) < D_g^G(r,\tau)$, which implies the scalar gradient field for case G is more intermittent than that for case R. This fact is consistent with the third observation of $\zeta_q^R > \zeta_q^G$ stated in Sec.1.

It is very interesting to attempt to explain the important problem; why does the geometry of intense structures of scalar gradient field depend on the large scale injection scheme? It seems to be so difficult to draw the definite conclusion for this problem at the present. Here we point out several important facts giving the hints for the further understanding of this problem, as follows.

- As shown in Fig.2, the strong intermittency of scalar increment in the ICR scale is due to the existence of cliffs or fronts, and closely related to the high intensity of fluctuation of θ. If the spatial

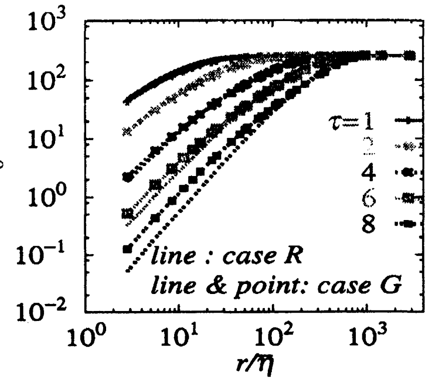

Figure 9: Comparison of $N_g(r,\tau)$ curves compensated by r^3 obtained by case G and R at $\tau = 1 \sim 8$.

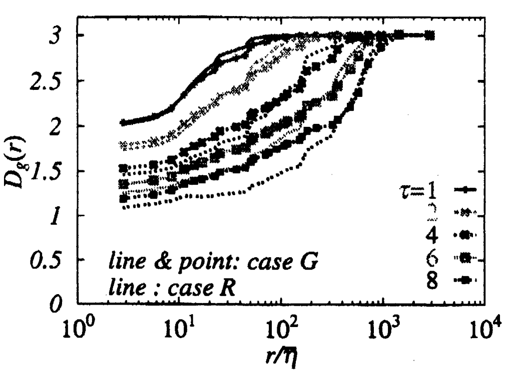

Figure 10: Comparison of local BCDs evaluated by Fig.9.

distributions of rare events of scalar is strongly dependent of the statistical details of external source, it is plausible that those of intense structures also depend on it.

- We should notice the theoretical and numerical facts that the passive scalar transfer is more nonlocal than that for energy [20]. This supports the idea that the small scale statistics of passive scalar is sensitive to the variation of large scale condition more than that of energy.

- It has been pointed out that the sheetlike structures (fronts) formed in the scalar dissipation field in 3D domain are unstable to the perturbation such as the external source [21], in which it is observed that instantaneous ζ_q^R at high order strongly varies with the temporal evolution. This implies that the life time of structures like the cliffs or fronts is a key to understand the different global structure between case G and R.

4.2 Intermittency exponents

We investigate the scaling of moment for the locally averaged dissipation field to get the further insight into the results shown in the previous subsection, where our analysis is restricted to the second order moment of them because the accuracy of statistics of the dissipation field obtained by the present DNS is ensured for their low order moments [17]. Kinetic energy dissipations based on the strain ϵ or vorticity Ω and the scalar variance dissipation χ are defined by

$$\epsilon(\mathbf{x},t) = 2\nu s^2, \quad \Omega(\mathbf{x},t) = \nu\omega^2, \quad \chi(\mathbf{x},t) = \kappa g^2, \tag{8}$$

where $\bar{\epsilon} = \bar{\Omega}$ for homogeneous turbulence. We consider the scaling behavior of the moment of the locally averaged dissipation field with volume $V_r = r^3$ defined by

$$S_q^z(r) = \langle z_r^q \rangle, \quad z_r(\mathbf{x}) = V_r^{-1} \int_{V_r} z(\mathbf{x}+\mathbf{x}')\, d\mathbf{x}', \tag{9}$$

where z denotes $z = \epsilon, \Omega$, or χ. Figure 11 shows $S_2^z(r)/S_1^z(r)^2$ curves for ϵ,Ω, and χ by cases G and R compensated by r^{μ_z}, where μ_z is called the intermittency exponent which is chosen to observe the wider plateau in the scaling range of $S_q^z(r)$ by eye. Observations yield the values of μ_z as

$$\mu_\epsilon \simeq \mu_\Omega \simeq 0.15, \quad \mu_\chi^R \simeq 0.27, \quad \mu_\chi^G \simeq 0.33. \tag{10}$$

From the results of Fig.11, we observe two facts that, i) the plateau is observed for χ clearer than those for ϵ and Ω with $\mu_{\epsilon,\Omega} < \mu_\chi$, ii) $\mu_\chi^R < \mu_\chi^G$, that is, the scalar dissipation for case G is more intermittent than that for case R as well as the scaling exponent of scalar structure function in ICR (see Fig.1). Observation i) is also comparable to the fact that the scalar structure function has the wider scaling range than that for velocity increment. Moreover observation ii) is consistent with the previous results

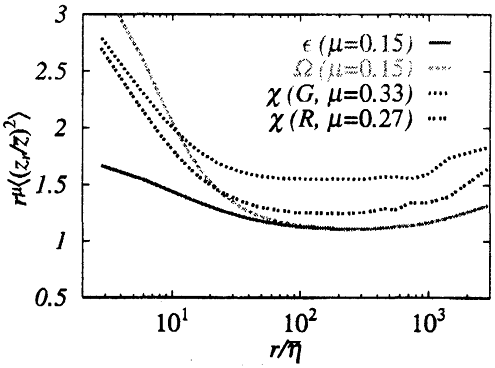

Figure 11: Comparison of the scaling behavior of compensated $S_2^z(r)/S_1^z(r)^2$ for the locally averaged dissipation fields.

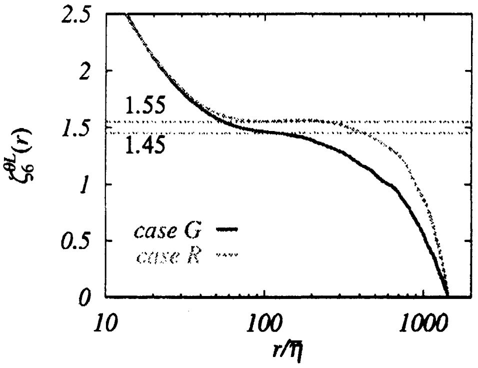

Figure 12: Comparison of local scaling exponents for scalar variance transfer flux between case G and R.

that the intense structure of scalar gradient for case G is more space filling (more intermittent) than that for case R. One should note that the values in eq.(10) are close to the experimental values $\mu_\epsilon \simeq 0.20 \pm 0.05$ and $\mu_\chi \simeq 0.34 \pm 0.05$ [22].

How are the values of μ_z related to the scaling exponents of ICR statistics? We consider the scaling law obtained by the refined similarity hypothesis of the energy cascade process [23] applied to the passive scalar transport. Cascading picture of the passive scalar analogous to the Kolmogorov theory implies that the fluctuation of χ_r is related to that of the transfer flux Π_r^θ in ICR as $\chi_r \sim \Pi_r^\theta$. Surrogate representation of Π_r^θ is given by using the velocity and scalar increments as $\hat{\Pi}_r^\theta \sim -\delta u_r \delta\theta_r^2/r$. So we expect that the scaling behavior of $\langle(\delta u_r \delta\theta_r^2)^2\rangle/r^2$ is same as that of $\langle\chi_r^2\rangle$. To follow this, we compute the mixed velocity scalar structure function and examine the scaling behavior by its local slopes. Results are shown in Fig.12. This clearly stands for $\langle(\hat{\Pi}_r^\theta)^2\rangle \sim r^{-\mu_f}$ with $\mu_f^R \simeq 0.45$ for case R and $\mu_f^G \simeq 0.55$ for case G, suggesting $\mu_f > \mu_\chi$, i.e. the scaling behavior of $\langle(\hat{\Pi}_r^\theta)^2\rangle$ is clearly different from that of dissipation field. Similar trend is also observed in the relation between ϵ_r and $\hat{\Pi}_r^u \sim -\delta u_r^3/r$.

It is interesting to discuss the another relation between the intermittency exponents and the scaling exponents of the fourth order scalar structure function. It is expected that the locally averaged scalar dissipation is dimensionally evaluated by $\chi_r \sim \kappa(\delta\theta_r/r)^2$ at smaller r. This implies the relation $\langle\chi_r^2\rangle/\langle\chi_r\rangle^2 \sim \langle\delta\theta_r^4\rangle/\langle\delta\theta_r^2\rangle^2$. That is, the scaling relation $\mu_\chi = 2\zeta_2^\theta - \zeta_4^\theta$ is suggested from the dimensional arguments. From the DNS data for the scaling exponent of scalar structure functions [7, 8], we can obtain $2\zeta_2^\theta - \zeta_4^\theta = 0.28$ for case R and 0.33 for case G. These are in good agreement with the estimations of intermittency exponent in eq. (10). This scaling relation has been clarified in the case for the Kraichnan model [24] and generalized to the q-th order moments as $\mu_q = q\zeta_2 - \zeta_{2q}$, which is also derived from it with $d \gg 1$ [25].

5 Conclusion

We discussed the geometric features of the vorticity, strain and scalar gradient fields by investigating the box counting dimensions of the level set of intense structures for them. Although the clear scaling behavior for evaluating D_0 is not observed for all cases of level set, the different behavior of the local BCDs suggest the existence of different geometry of intense structures among each fields. We found that the scalar gradient field is more space filling than the vorticity and strain fields at high intensity of fluctuation. This is consistent with the observation that the passive scalar field is more intermittent than the velocity one. Moreover the saturation of the scaling exponent of the scalar structure function for case G was explained in terms of the geometric feature of the intense structures of the scalar gradient field, where it was shown that the lower bound of BCDs is related to the saturation value of ζ_q^G at high order.

Influence of the large scale condition on the scalar dissipation statistics was also investigated by comparing the results for both cases G and R. We showed that the geometrical dimension of the intense structure of scalar gradient is dependent of the scalar injection scheme, where it was obtained that the level set by case G is more space filling than that of case R. This fact implies that case G is more intermittent than case R, as shown in Fig.1. Further analysis was carried out by investigating the scaling behavior of locally averaged dissipation statistics. We showed that the intermittency exponent of scalar dissipation evaluated by case G is larger than that by case R, suggesting the stronger intermittency of case G than that of case R. These results are everything consistent with the third observation in Sec.1.

Acknowledgements

The authors thank the Earth Simulator Center, the Theory and Computer Simulation Center of the National Institute for Fusion Science, and the Information Technology Center of Nagoya University for providing the computational resources. T. W. is supported by the Grant-in-Aid for Scientific Research No.17760139 in the Ministry of Education, Culture, Sports, Science and Technology of Japan.

References

[1] A. M. Obukhov, Izv. Akad. Nauk. SSSR. Geophr. Geofiz **13**, 58 (1949).

[2] S. Corrsin, J. Appl. Phys. **22**, 469 (1951).

[3] Z. Warhaft, Annu. Rev. Fluid Mech. **32**, 203 (2000).

[4] A. Gylfason and Z. Warhaft, Phys. Fluids **16**, 4012 (2004).

[5] A. Celani, A. Lanotte, A. Mazzino, and M. Vergassola, Phys. Rev. Lett. **84**, 2385 (2000).

[6] A. Celani, A. Lanotte, A. Mazzino, and M. Vergassola, Phys. Fluids **13**, 1768 (2001).

[7] T. Watanabe and T. Gotoh, New J. Phys. **6**, 40 (2004). (http://stacks.iop.org/1367-2630/6/40)

[8] T. Watanabe and T. Gotoh, submitted to Phys. Fluids (2006).

[9] R. H. Kraichnan, Phys. Rev. Lett. **72**, 1016 (1994); Phys. Rev. Lett. **78**, 4922 (1997).

[10] B. I. Shraiman and E. D. Siggia, Nature **405**, 639 (2000).

[11] G. Falkovich, K. Gawedzki and M. Vergassola, Rev. Mod. Phys. **73**, 913 (2001).

[12] F. Moisy and J. Jiménez, J. Fluid Mech. **513**, 111 (2004).

[13] T. Gotoh, D. Fukayama and T. Nakano, Phys. Fluids **14**, 1065 (2002).

[14] P. K. Yeung, D. A. Donzis and K. R. Sreenivasan, Phys. Fluids **17**, 081703 (2005).

[15] A. M. Yaglom, Dokl. Akad. Nauk SSSR **69**, 743 (1949).

[16] F. Moisy, H. Willaime, J. S. Andersen and P. Tabeling, Phys. Rev. Lett. **86**, 4827 (2001).

[17] T. Watanabe and T. Gotoh, to appear in Proceedings of IUTAM symposium on Elementary vortices and coherent structures: Significance in turbulence dynamics.

[18] G. Brethouwer, J. C. R. Hunt, and F. T. M. Nieuwstadt, J. Fluid Mech. **474**, 193 (2003).

[19] Wm. T. Ashurst, A. R. Kerstein, R. M. Kerr, and C. H. Gibson, Phys. Fluids **30**, 2343 (1987).

[20] T. Gotoh and T. Watanabe, J. Turbulence **6**, N33 (2005).

[21] S. Chen and N. Cao, Phys. Rev. Lett. **78**, 3459 (1997).

[22] C. Meneveau, K. R. Sreenivasan, P. Kailasnath, and M. S. Fan, Phys. Rev. A **41** 894 (1990).

[23] A. N. Kolmogorov, J. Fluid Mech. **13**, 82 (1962).

[24] S. Chen and R. H. Kraichnan, Phys. Fluids **10**, 2867 (1998).

[25] M. Chertkov and G. Falkovich, Phys. Rev. Lett. **76**, 2706 (1996).